CERN 70-16
Health Physics Group
27 May 1970

CERN 70-16

ORGANISATION EUROPÉENNE POUR LA RECHERCHE NUCLÉAIRE
CERN EUROPEAN ORGANIZATION FOR NUCLEAR RESEARCH

RADIATION MEASUREMENTS AROUND A BEAM STOPPER IRRADIATED BY 19.2 GeV/c PROTONS, AND NEUTRON ENERGY SPECTRA FROM MONTE CARLO NUCLEON-MESON CASCADE CALCULATIONS

K. Goebel and J. Ranft*)

G E N E V A

1970

---

*) Rutherford High-Energy Laboratory, Didcot, Berkshire, England.

CERN 70-16
Health Physics Group
27 May 1970

ORGANISATION EUROPÉENNE POUR LA RECHERCHE NUCLÉAIRE
CERN EUROPEAN ORGANIZATION FOR NUCLEAR RESEARCH

RADIATION MEASUREMENTS AROUND A BEAM STOPPER IRRADIATED BY 19.2 GeV/c PROTONS, AND NEUTRON ENERGY SPECTRA FROM MONTE CARLO NUCLEON-MESON CASCADE CALCULATIONS

K. Goebel and J. Ranft*)

GENEVA

1970

---

*) Rutherford High-Energy Laboratory, Didcot, Berkshire, England.

ABSTRACT

Flux density measurements around a 300-cm-long steel beam stopper are made by using activation detectors with different energy thresholds. These measurements, from 21 positions inside and 10 outside the shielding tunnel, provide information on the radiation at these positions, the spectrum of secondary neutrons, and attenuation by and shielding efficiency of the beam stopper and the concrete shielding tunnel, respectively. Calculations using a Monte Carlo method are made to evaluate the flux densities and spectra above 100 MeV. These calculations and the experimental data are compared, and it is shown that both agree in general within a factor of 2.

CONTENTS

1. INTRODUCTION

Beam areas of primary and secondary high-energy particles are often protected by interlocked beam stoppers or beam plugs. The radiation field in the surroundings of such beam stoppers and their attenuation efficiency are of primary concern for the layout of particle beams and their shielding. In order to solve some acute problems connected with transferring the beam from the CERN Proton Synchrotron (CPS) to the new intersecting storage rings, flux densities and dose measurements were made around a beam stopper in a fast-ejected primary proton beam.

In the past, attenuation measurements and shielding calculations were made in various materials in the forward directions[1-3]. In this case, the geometry is such that the lateral dimensions of the absorber are large compared with the cross-sections of the incoming beam and of the particle cascade developing inside the absorber. Other measurements and calculations are concerned with the transverse attenuation in configuration such as beam tunnels or a lateral shielding wall[4-7]. The experiment reported here combines some of the features of the two simple cases: a long but narrow (compared with the particle cascade) steel beam plug, and a shielding tunnel all around this radiation source.

We were interested in checking whether the Monte Carlo method could also predict with some reliability (as in the former calculations) the fluxes around the beam stopper and outside the transverse concrete shielding.

The Monte Carlo method reveals information primarily about the star density inside the steel and the concrete. In former shielding experiments, nuclear emulsions were used to measure the star density, so direct comparison between experiment and calculation was possible. However, the emulsion technique requires considerable scanning effort, and the method is somewhat remote from the standard technique used in health physics. As the beam-stopper measurements and calculations are of practical interest for radiation protection, it seems desirable to use the same methods as those normally applied for assessing the flux density and dose levels in areas occupied by workers. Therefore we used for the measurements such activation detectors as plastic scintillators, sulfur, aluminium, and moderated and bare indium.

In order to compare the results from the activation detectors with the star densities and the fluxes at energies above 100 to 200 MeV, the spectrum of the particles producing the activity in the detector must be known. Spectral information is readily obtained from the activation detectors, if detectors with responses to different parts of the energy range of interest are used. This is the case with our detectors up to about 100 MeV. (We could not measure with sufficient sensitivity ^{149}Tb activity produced in gold or mercury, which has a threshold at 600 MeV.) Above this energy the spectral shape is calculated by the Monte Carlo method. The flux densities obtained from the activation detectors, at 19 positions inside the shielding tunnel and 10 positions outside the shield, were compared with the predictions from the Monte Carlo calculations. The fact that both agree within acceptable limits strengthens the confidence that even in more complicated geometries the Monte Carlo calculation can predict flux densities for new shielding layouts.

2. EXPERIMENTAL LAYOUT; MEASUREMENTS OF PARTICLE FLUXES

Two large standard steel beam stoppers, 1.50 m long and 30 cm in diameter, were installed in the e_4 beam tunnel. In this fast-ejected proton beam, particle losses upstream from the selected site could be expected to be small, as the primary proton beam has small geometrical dimensions in the fast-ejected mode. The beam stopper is therefore the principal radiation source. At the chosen position, the shielding of the tunnel was without cracks or inhomogeneities; the shielding thickness at the right (south) side of the tunnel was 80 cm less than on the top and on the north side (Fig. 1).

In the flux-density measurements, a number of activation detectors with different thresholds were used. Table 1 shows the main characteristics of the detectors. The detectors were placed inside the tunnel in order to obtain particle flux-density patterns around the beam stopper (Series I), and outside on the shielding surface to measure the efficiency of the transverse shielding at large angles (Series II). For Series I, the choice of a measuring site was limited by the space available inside the shielding tunnel. The positions for flux and density measurements are indicated in Fig. 2.

The exposures were organized so as to comply with the requirements of the activity measurements in three short exposures, A_0, B_0, and C_0, of 23 sec (= 10 PS pulses) each for short half-lives, and three longer exposures of 20 min each for the long half-lives. During the exposure the beam intensity was continuously monitored by a current transformer and a secondary-emission chamber (SEC). The calibration of the SEC was based on the

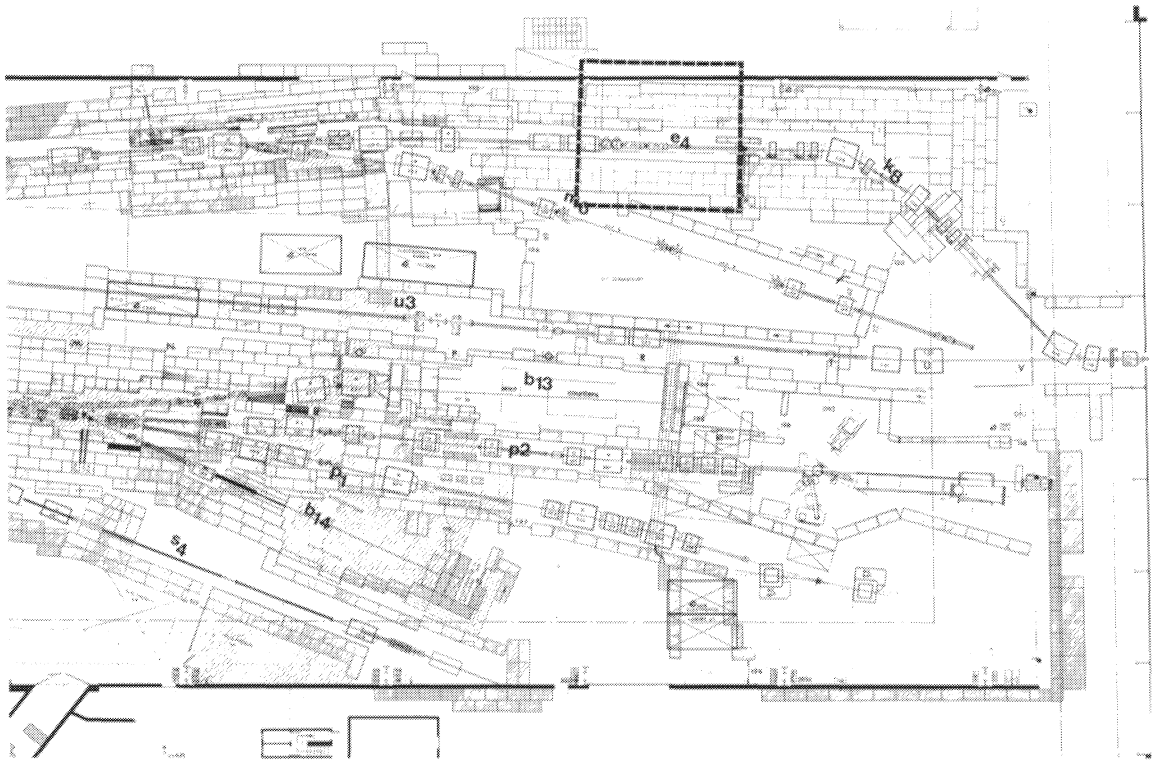

Fig. 1 The experimental area inside the CERN-PS East Hall (March 1968).

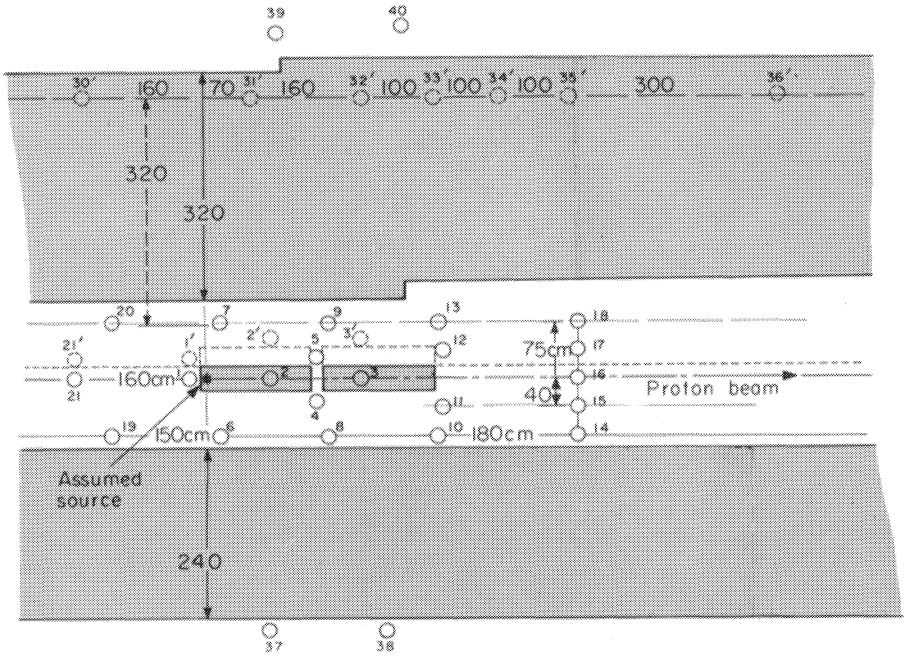

Fig. 2 The measuring sites inside (positions 1 to 21) and outside (positions 30 to 40) the proton beam tunnel. The broken lines indicate the vertical section, which is turned by 90° into the horizontal plane.

Table 1

Activation detectors used for flux density measurements

Detector	Reaction	Energy range (MeV)	Cross-section (mb) (at energy in MeV)	Decay mode	Half-life	Detector size
Bare indium	$^{115}In(n,\gamma)^{116m}In$	thermal energy	200,000 (thermal energy)	γ,β^-	54 min	48 mm ϕ 0.3 mm thick
Indium in moderator	$^{115}In(n,\gamma)^{116m}In$	0.1-10	--- ---	γ,β^-	54 min	48 mm ϕ 0.3 mm thick
Sulphur	$^{32}S(n,p)^{32}P$	2.3-20	300(10)	β^-	14.1 d	48 mm ϕ 5 mm thick
Aluminium	$^{27}Al(n,\alpha)^{24}Na$	6.7 →	120(14)	β^-,γ	900 min	0.1-10 kg
	$^{27}Al(x,x2pn)^{24}Na$	35 →	14(50)	β^-,γ	900 min	0.1-10 kg
Plastic scintillator	$^{12}C(n,2n)^{11}C$	20 →	22(200)	β^+	20 min	Up to 10 cm ϕ 10 cm high
	$^{12}C(x,xn)^{11}C$	20 →	30(200)	β^+	20 min	Up to 10 cm ϕ 10 cm high
Aluminium	$^{27}Al(x,x2p3n)^{22}Na$	45 →	20(200)	β^+,γ	2.64 years	0.1-10 kg

Al-^{24}Na reaction cross-section (carried out by Dr. L. Hoffmann, MPS Division, CERN). Eventual systematic errors in the absolute cross-section values would be the same for the secondary flux measurements. Table 2 gives the monitor readings for the exposures A_0 to F_0. The average proton current was 3.1 to 3.4 $\times 10^{11}$ p/sec. All the results were normalized to 10^{12} p/sec, so the actual secondary fluxes measured were lower by a factor of 3 than the results given below.

Table 2

Primary beam monitor results (at proton energy 18.4 GeV)

Exposure	Time	Current transformer	Secondary emission chamber	Charge loss monitor	Average flux into beam stopper p/sec
A_0	23 sec	7.08×10^{12}	7.08×10^{12}	6.85×10^{12}	3.05×10^{11}
B_0	23 sec	7.87×10^{12}	7.90×10^{12}	7.97×10^{12}	3.43×10^{11}
C_0	23 sec	7.60×10^{12}	7.84×10^{12}	7.55×10^{12}	3.33×10^{11}
D_0	23 min	448×10^{12}	461×10^{12}	---	3.30×10^{11}
E_0	30.7 min	559×10^{12}	580×10^{12}	---	3.10×10^{11}
F_0	23 min	447×10^{12}	466×10^{12}	---	3.33×10^{11}

The results of the activation detector measurements are basically specific activities of certain isotopes in the detectors. If we assume an average cross-section, the specific activity can be interpreted as flux density. Table 3 gives a summary of all results. The cross-sections assumed for deriving the flux densities are given at the head of each column. [More details have been given elsewhere[8].] Figures 3 and 4 show the high-energy particle densities [^{12}C(x,xn)^{11}C] inside and outside the shield, respectively, normalized to 1 m distance by multiplying by r^2 (where r is in metres).

Counting errors for all samples except the ^{32}P and ^{22}Na are low: $\leq 10\%$. The results are, however, influenced by small inhomogeneities in the shield, and by positioning errors that might be important inside the tunnel where the radiation field has large gradients. Detectors exposed side by side in the "same" position can thus "see" different flux densities.

3. EXPERIMENTAL NEUTRON SPECTRA

The production cross-section of the isotopes used in the activation detector system is known for most of the strongly interacting particles over the whole energy range ($\leq$ 30 GeV). As excitation or response functions, we applied the curves given by Charalambus et al., and by Cumming[9]. A specific decay or counting rate found in a measurement is proportional to

$$DR_{det} \quad \text{or} \quad CR_{det} \approx \int R(E)_{det} \times \phi(E)\, dE \ ,$$

Table 3

Results from activation detectors and dosimeters. Series I (inside tunnel pos. 1-21; Series II (outside concrete shield) pos. 30-40. (HEP = high-energy particles; FN = fast neutrons; Th N = thermal neutrons).

Position	Direction	Distance d^2 (m)	Shielding (g/cm^2)	Flux density (neutrons/cm^2-sec)					
				HEP ^{11}C (22 mb)	HEP ^{22}Na (20 mb)	FN (14 MeV) ^{24}Na (120 mb)	FN (10 MeV) ^{32}P (300 mb)	FN In mod. 10.5 cmp (n/cm^3 sec)	Th N In 20 cpm (n/cm^2 sec)
1	up	0.137		355×10^8	118×10^6	132×10^6	322×10^6	596×10^6	
2	up	1.10		281×10^8	185×10^6	104×10^6	174×10^6	561×10^6	
3	up	4.66		54×10^8	^{6}	10×10^6	21×10^6	489×10^6	
4	r	2.40		88×10^8	30×10^8	26×10^6	49×10^6	542×10^6	
5	ℓ	2.40		110×10^8	33×10^6	28×10^6	48×10^6	544×10^6	
6	r	0.67		165×10^8	68×10^6	67×10^6	168×10^6	519×10^6	
7	ℓ	0.67		205×10^8	81×10^6	83×10^6	210×10^6	522×10^6	
8	r	3.43		82×10^8		25×10^6	48×10^6	361×10^6	
9	ℓ	3.43		91×10^6	65×10^8	27×10^6	46×10^6	367×10^6	
10	r	10.5		18×10^6		5.6×10^6	11×10^6	290×10^6	
11	ℓ	10.5		9.7×10^6		4.0×10^6	9.4×10^6	283×10^6	
12	ℓ	10.5		8.4×10^8		3.7×10^6	7.9×10^6	284×10^6	
13	ℓ	10.5		21×10^6		5.7×10^6	10×10^6	289×10^6	
14	r	26.8		5.4×10^6		1.5×10^6	1.5×10^6	108×10^6	
15	r	26.5		4.0×10^6		1.4×10^6	2.8×10^6	111×10^6	
16	±0	26.2		3.4×10^6		1.4×10^6	2.8×10^6	118×10^6	
17	ℓ	26.5		3.5×10^6		1.5×10^6	3.1×10^6	117×10^6	
18	ℓ	26.8		4.9×10^6		1.8×10^6	3.2×10^6	114×10^6	
19	r	2.3		8.6×10^6		4.4×10^6	14×10^6	42×10^6	
20	ℓ	2.3		7.4×10^6		4.5×10^6	14×10^6	42×10^6	
21	up	3.43		3.4×10^6		4.0×10^6	9.3×10^6	33×10^6	
30	up	18.7	770	3260		935		2830	762
31	up	16.0	770	10500		2980		8120	2000
32	up	20.3	770	3900		935		2130	600
33	up	25.0	770	1840		437		1870	352
34	up	32.2	770	670		198		1020	121
35	up	41.0	770	210		87		640	149
36	up	77.5	770	3.8		9.7		362	95
37	r	12.6	580	26300		9250		53300	14550
38	r	18.1	580	9340		3150		49500	6920
39	ℓ	27.0	770	3830		1330		6890	1340
40	ℓ	33.0	820	2590		868		4950	1150

where $R(E)_{det}$ is the response or excitation function of the detector, and $\phi(E)$ is the differential energy spectrum of neutrons. For simplicity, the response functions for neutrons are used, as neutrons represent the predominant particle group, at least in the energy range where the detectors are most sensitive.

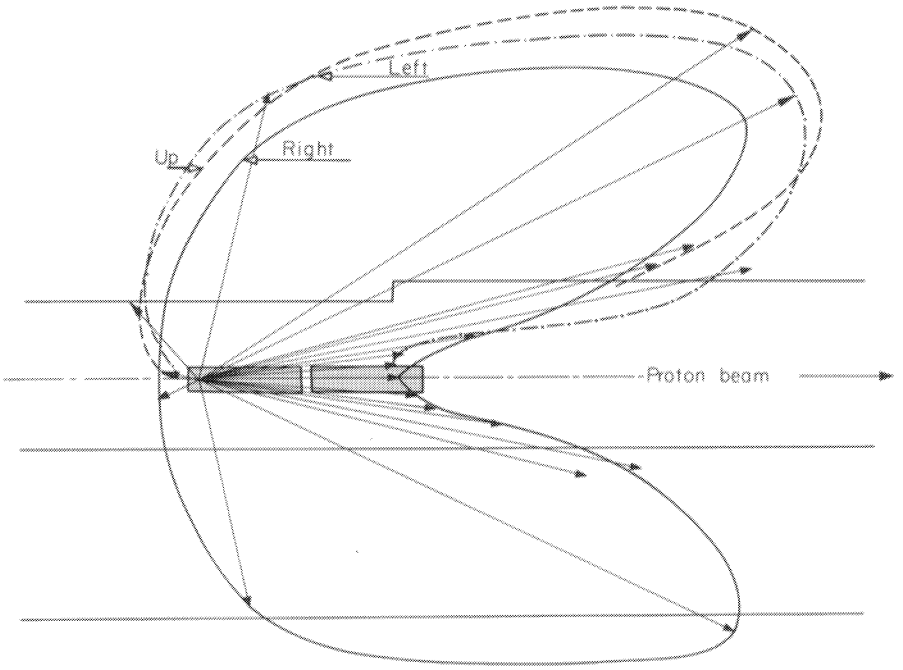

Fig. 3 High-energy particle flux densities around the beam stopper. The lengths of the arrows correspond to the flux density reduced to 1 m distance ($1/r^2$) from the assumed source (inside the first stopper).

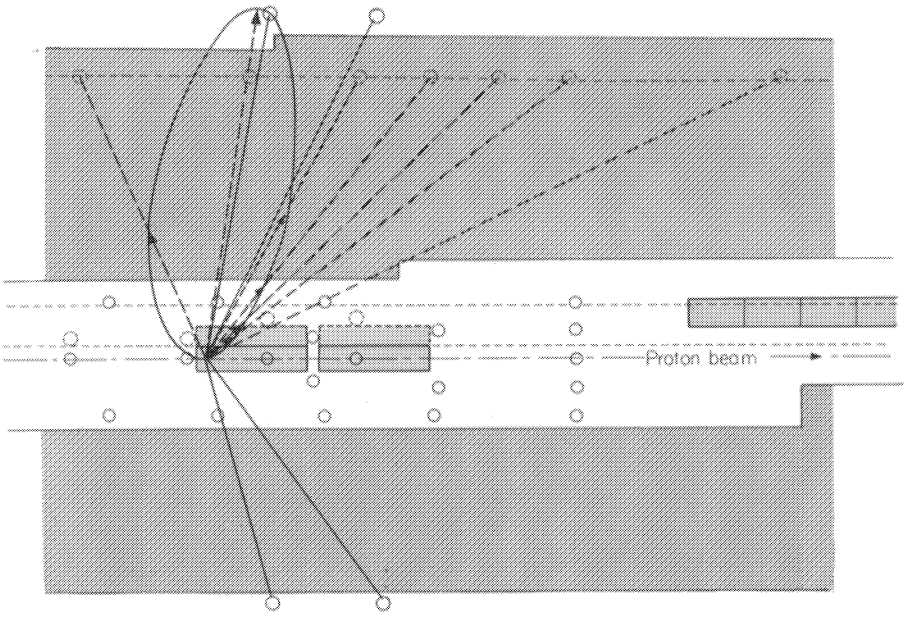

Fig. 4 High-energy particle flux densities measured on top of the shielding. The lengths of the arrows are proportional to the flux densities reduced by 1 m distance from the assumed source. The maximum flux is measured at 80° with the beam direction.

When, as in our case, more than one activation detector is used, the different $R(E)_{det}$ provide information about the spectrum. From Table 1 we see that the spectrum is reasonably well determined at thermal energies, in the range of fast neutrons of 0.1 to 20 MeV and up to about 100 MeV. By calculating the products $R(E_i) \times \phi(E_i)$ for different energy intervals E_i and summing them up, we can calculate the DR's from conjectured spectra. By modifying the spectrum in repeated trails we finally find a spectrum that gives a response equal to the measured one. Such a spectrum is not completely determined, and the method does not reveal a unique answer; however, a smooth spectrum that is free from oscillations, and matches the counting rates, might be considered a "reasonable" spectrum.

The program TELLY computes counting rates that would be observed from a given spectral distribution. (TELLY was originally written by Marjorie Simmons, Nickey Little, and Alan Smith to find the spectra in the CERN-Rutherford-Berkeley shielding experiments from the responses of the same detectors.) TELLY employs an open-loop technique to solve the problem, in the sense that the user must supply modifications to an input neutron spectrum in order to achieve the match with a set of observed count rates. As written, the program will not generate new trial spectra automatically in order to seek the desired match conditions. The light-pen is used as the means for modifying spectral shapes. One simply draws a desired modification on the cathode-ray tube display, and almost instantly can observe the changes in calculated detector count rates brought about by this special alteration.

A similar approach was made by applying the LOUHI program[10]. Using an iteration process starting from a conjectured spectrum, this program finds a spectrum with the least-square deviations between calculated and measured responses. Above 100 MeV the spectra are ambiguous and not well determined by the detectors used. From the Monte Carlo calculations discussed in the next paragraph we have information about the spectra at higher energies. By imposing this spectral distribution above 100 MeV, the TELLY and LOUHI programs can still match the detector responses at lower energies. Examples of such experimental spectra are given in Fig. 5. In Table 4 the difference between measured responses and those calculated by the LOUHI program are given. Most of the spectra obtained match the responses within a few per cent, the highest difference being about 40%.

In Fig. 5e the spectra for different positions inside the tunnel and outside the concrete shield are compared with each other. Some characteristic changes can be observed when the site of the measurement moves downstream in the beam direction: at a distance of about 75 cm from the beam axis, the spectra upstream from the impact point (position 19) have very high contributions of low-energy neutrons. At energies above 1 MeV the spectra decrease very quickly. There are almost no high-energy particles above 100 MeV. As we move to positions 6 and 8, small shoulders build up in the spectrum at about 100 MeV. This shows, as expected, the increasing number of particles of higher energy scattered and produced in the more forward direction. This systematic change continues at positions 10 and 14, where the forward-scattered particles become more and more pronounced.

When comparing the spectra outside the shield we have, starting with position 31 (at the same longitudinal position as the beam stop impact point), a spectrum with a flat region between 1 and 100 MeV. In the Monte Carlo calculations discussed below, this flat

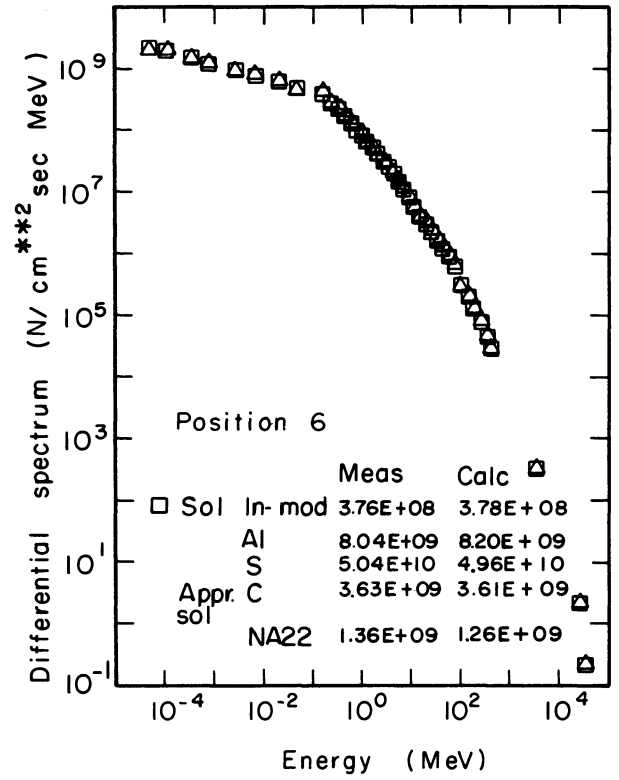
Differential spectrum (N/ cm**2 sec MeV)
Position 6
Meas Calc
□ Sol In-mod 3.76E+08 3.78E+08
Al 8.04E+09 8.20E+09
S 5.04E+10 4.96E+10
Appr. C 3.63E+09 3.61E+09
sol
NA22 1.36E+09 1.26E+09
Energy (MeV)

a)

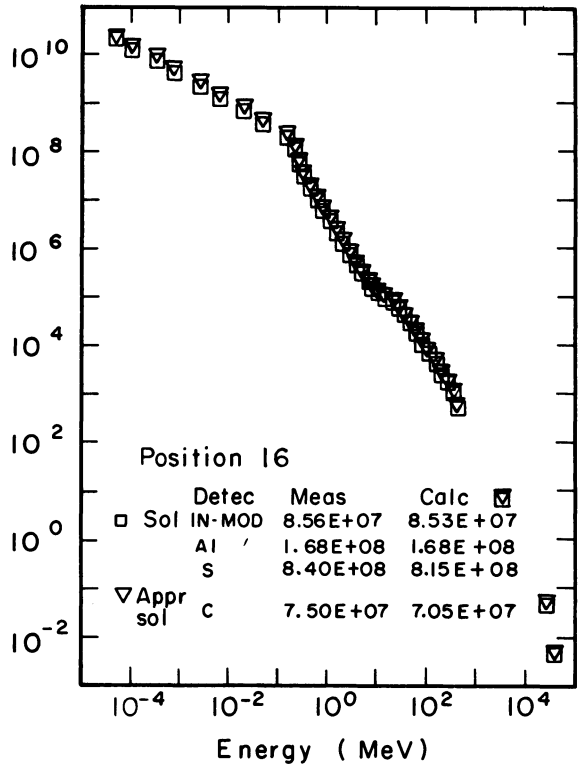
Position 16
Detec Meas Calc
□ Sol IN-MOD 8.56E+07 8.53E+07
Al 1.68E+08 1.68E+08
S 8.40E+08 8.15E+08
▽Appr sol C 7.50E+07 7.05E+07
Energy (MeV)

b)

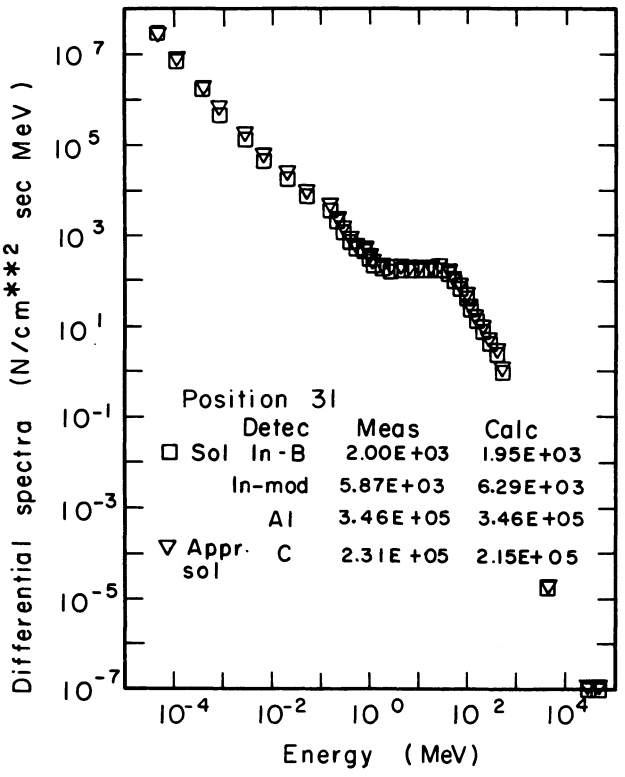
Differential spectra (N/cm**2 sec MeV)
Position 31
Detec Meas Calc
□ Sol In-B 2.00E+03 1.95E+03
In-mod 5.87E+03 6.29E+03
Al 3.46E+05 3.46E+05
▽Appr sol C 2.31E+05 2.15E+05
Energy (MeV)

c)

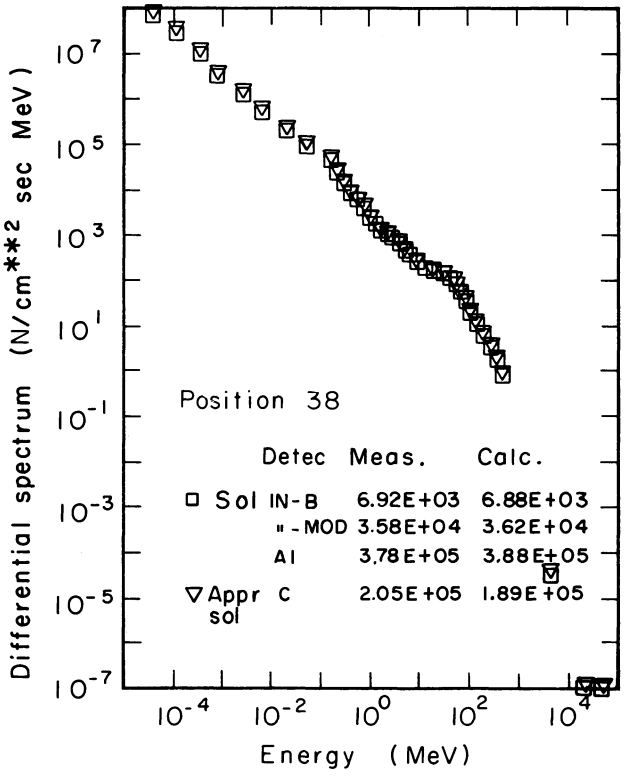
Differential spectrum (N/cm**2 sec MeV)
Position 38
Detec Meas. Calc.
□ Sol IN-B 6.92E+03 6.88E+03
" -MOD 3.58E+04 3.62E+04
Al 3.78E+05 3.88E+05
▽Appr sol C 2.05E+05 1.89E+05
Energy (MeV)

d)

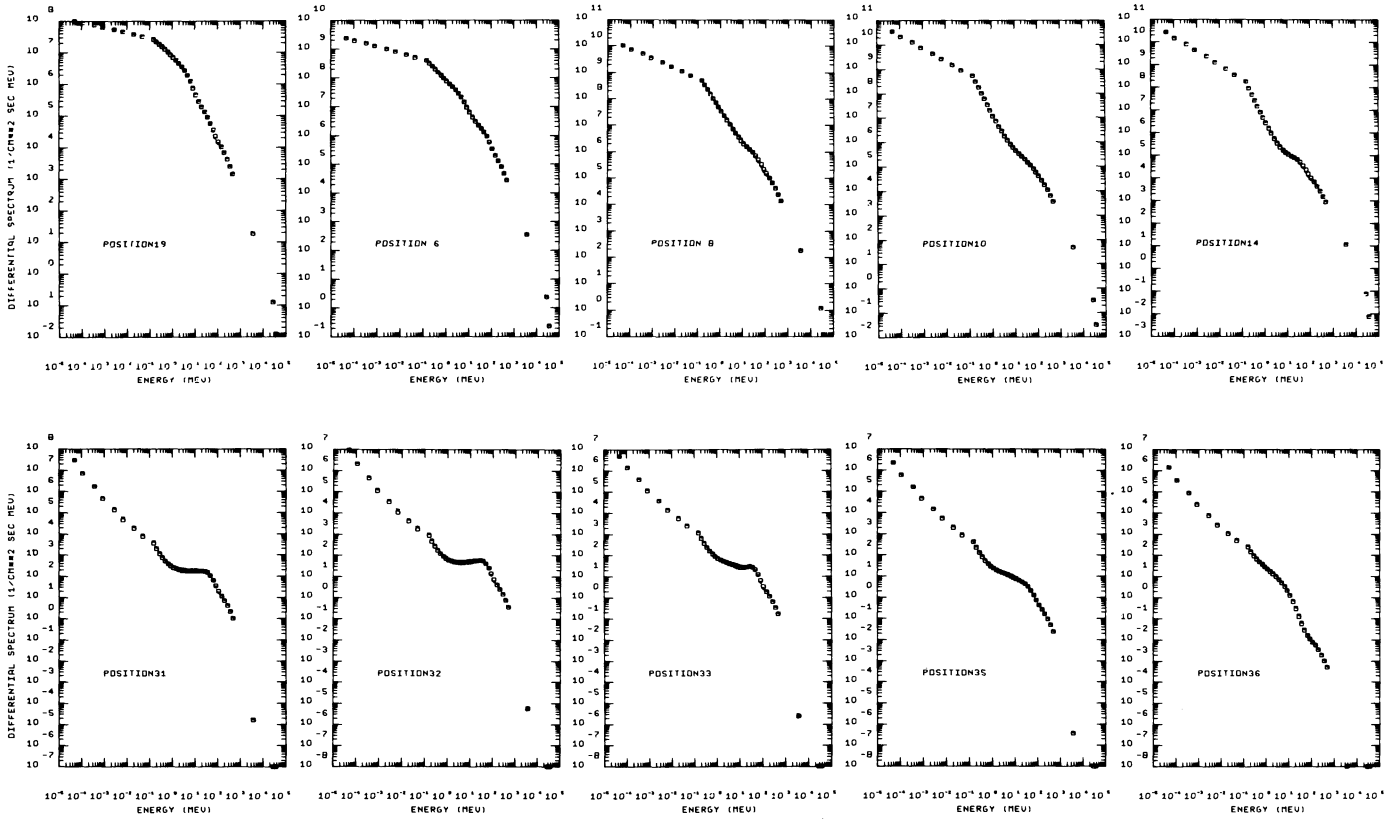

Fig. 5 Neutron spectra as calculated with the LOUHI program. Two spectra are from positions inside the tunnel (Figs. 5a and 5b); two are from outside (Figs. 5c and 5d), at the points of maximum radiation: on top of the shield of position 31, and from the side, where the shielding is only 240 cm of concrete, at position 38. Figure 5e is a comparison of spectra taken inside the tunnel and outside the shield along the beam line.

region of the spectrum does not show up, as the Monte Carlo particle spectrum has a lower energy cut-off at about 100 MeV. The flat part almost becomes a peak at positions 32 and 33, but disappears as one moves to more downstream positions (35 and 36). This shows that the greater shielding thickness, which the radiation must penetrate toward the downstream positions, attenuates the secondary particles more than the flux density increases at smaller angles. The highest dose-rates and also the largest relative contribution to the dose-rate from high-energy particles are found at angles that are between 70° and 90° to the beam direction.

4. NEUTRON ENERGY SPECTRA ABOVE E = 100 MeV FROM MONTE CARLO NUCLEON-MESON CASCADE CALCULATIONS

The Monte Carlo nucleon-meson cascade calculations in a block of shielding material, and the computer program TRANSK, were described in Refs. 3 and 6. New experimental data and other improvements were recently introduced[11]. These improvements include:

i) an improved formula for multiparticle production, which was fitted to new experimental data;

ii) energy-dependent absorption cross-sections for strongly interacting particles on nuclei;

Table 4

Ratio of (CR-CM) × 100/CM [CR = responses of activation detectors (LOUHI program), CM = responses from activation measurement; ±0 = difference less than 1%; -- = no measurements made.]

Position	Activation detector					
	Indium		^{24}Na	^{32}P	^{11}C	^{22}Na
	Bare	Moderated				
Inside tunnel						
1	--	±0	+4	-4	-8	-1
2	--	±0	-4	+2	+1	-34
3	--	±0	+2	±0	-28	-25
4	--	±0	+2	±0	-7	+2
5	--	±0	+2	±0	-9	+8
6	--	±0	+2	-2	±0	-7
7	--	+1	+3	-2	-2	-5
8	--	±0	±0	±0	-10	--
9	--	±0	-3	+2	+5	-35
10	--	±0	±0	±0	±0	--
11	--	±0	±0	±0	-7	--
12	--	±0	±0	±0	-6	--
13	--	±0	±0	+2	-12	--
14	--	±0	-1	+3	-12	--
15	--	±0	±0	+1	-8	--
16	--	±0	±0	+1	-6	--
17	--	±0	±0	+1	-5	--
18	--	±0	±0	+2	-10	--
19	--	+1	+2	-2	-5	--
20	--	+1	+3	-2	-5	--
21	--	+1	-3	+2	+3	--
Outside shielding						
30	-5	+15	±0	--	-2	--
31	-2	+7	±0	--	-7	--
32	-4	+10	±0	--	-9	--
33	-1	+4	+3	--	-10	--
34	±0	+2	+2	--	-8	--
35	±0	+3	±0	--	-3	--
36	-2	+4	±0	--	+3	--
37	±0	+4	±0	--	-5	--
38	±0	7	-3	--	+8	--
39	±0	+3	±0	--	-6	--
40	±	+3	±0	--	-6	--

iii) a better representation of ionization energy losses and nuclear excitation energies;

iv) an improved treatment of energy conservation in the cascade, and introduction of a lower cut-off momentum or energy that can be changed but is usually around E_{cu} = 50 to 125 MeV;

v) separate calculations of star and track densities, and more reliable calculation of the energy deposited by the cascade.

The program TRANSK was further modified to calculate the energy spectra of protons, neutrons, and pions as functions of the radial distance r from the beam axis in the shielding block or as functions of the depth z in the shielding block. Figures 6 to 8 give calculated proton, neutron, and pion energy spectra for different radii r in an iron block. The cascade was excited by a 20 GeV/c proton beam. The neutrons are the most important components in the cascade. It is difficult to compare these curves with corresponding experimental particle spectra. Cosmic-ray neutron spectra are expected to be different in the region of the high energies considered. The primary spectrum is different and extends to much higher energies than 20 GeV, and the same must be true for the neutron spectra at sea level. Neutron energy spectra around accelerators, evaluated from activation detector measurements as in the preceding section, cannot be expected to be significant much above E = 100 MeV even if the curves are continued up to much higher energies, as was done in Ref. 5. There seems to be no physical process that could be responsible for the transmission, through thick lateral shields, of neutrons with energies nearly equal to the primary proton energy, but many such neutrons are present according to the spectra in Ref. 5. There is no direct experimental evidence available for the presence of these high-energy neutrons at the positions considered.

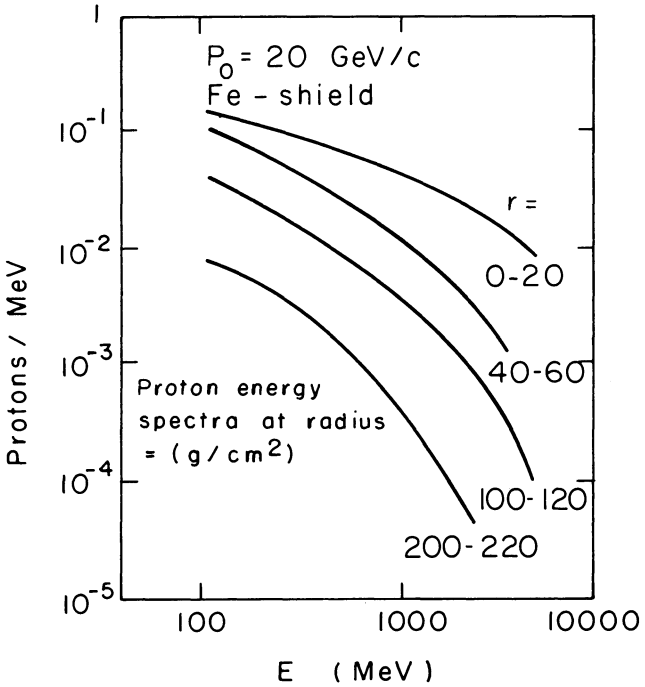

Fig. 6 Calculated proton energy spectra in a block of iron for different radial distances from the primary proton beam line.

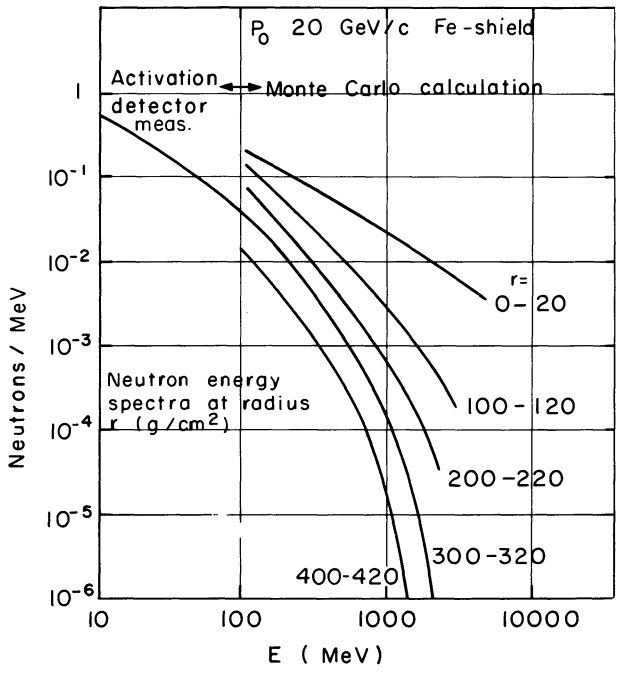

Fig. 7 Calculated neutron energy spectra in a block of iron for different radial distances from the primary proton beam line. The curve for r = 300 to 320 g/cm^2 is continued down to E = 10 MeV by using the ring-top neutron spectrum of Ref. 5.

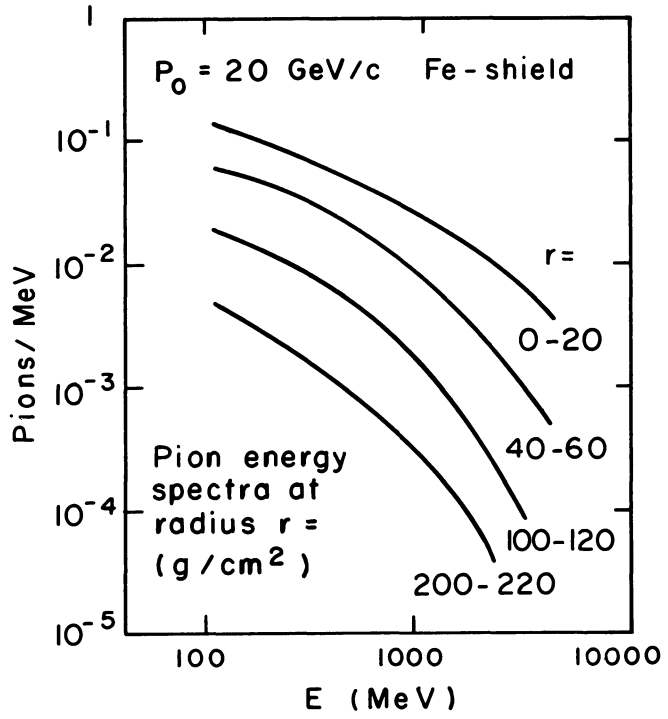

Fig. 8 Calculated pion energy spectra in a block of iron for different radial distances from the primary proton beam line.

Below 100 MeV however, the experimental neutron spectra are expected to be much better, and we use the spectra shown in the preceding section to continue the calculated energy spectra from E = 100 MeV (about the lowest energy for which the spectra can at present be calculated) down to lower energies. This was done with typical activation detector spectra for one of the curves in Fig. 7.

5. CALCULATIONS OF STRONGLY INTERACTING PARTICLE FLUXES IN AND AROUND THE BEAM STOPPER

The Monte Carlo nucleon-meson cascade calculation[3,6,10] was first developed for applications in the simplest geometrical situation. The underlying principles and the physical data used have now been shown to lead to results in agreement with measurements in the simple geometric situation. Therefore we can now apply the same method to more complicated geometrical situations. The first such applications have already been reported in Ref. 7. Here we consider a geometric situation similar to that around the beam stopper.

The primary proton beam hits a cylindrical iron beam stopper of radius r_0 and length ℓ_1, surrounded by a cylindrical concrete shield with inner radius r_s. The computer program KASTRA calculates, for the time being, only the proton, neutron, and pion star densities inside the beam stopper and in the concrete shield. However, we need the flux densities to compare them with the activation detector measurements. The assumption made here is that the flux densities inside the steel or concrete are proportional to the calculated star densities. This would be correct only in a calculation with cross-sections independent of energy and type of particle. We know, however, from the results of the program TRANSK that the assumption is a good approximation.

The resulting flux density for all strongly interacting particles, normalized to one incoming primary proton, is given in Fig. 9. The calculations were made with r_0 = 15 cm, ℓ = 300 cm, and r_s = 75 cm. The neutron, proton, and pion fluxes at r_s = 75 cm in the shield are compared in Fig. 10. The neutrons are by far the most important component.

It is very difficult to get statistically significant results at large radii in the concrete shield. Therefore we calculate also the mean transverse attenuation of the flux density in the concrete by integrating over all z-values considered. The histogram obtained is given in Fig. 11. The transverse attenuation of the flux density $\phi(r,z)$ is well represented by

$$\phi(r,x) \approx \exp\left(-r/\lambda_r\right) \quad ,$$

with λ_r = 80 g/cm^2 for the layout studied.

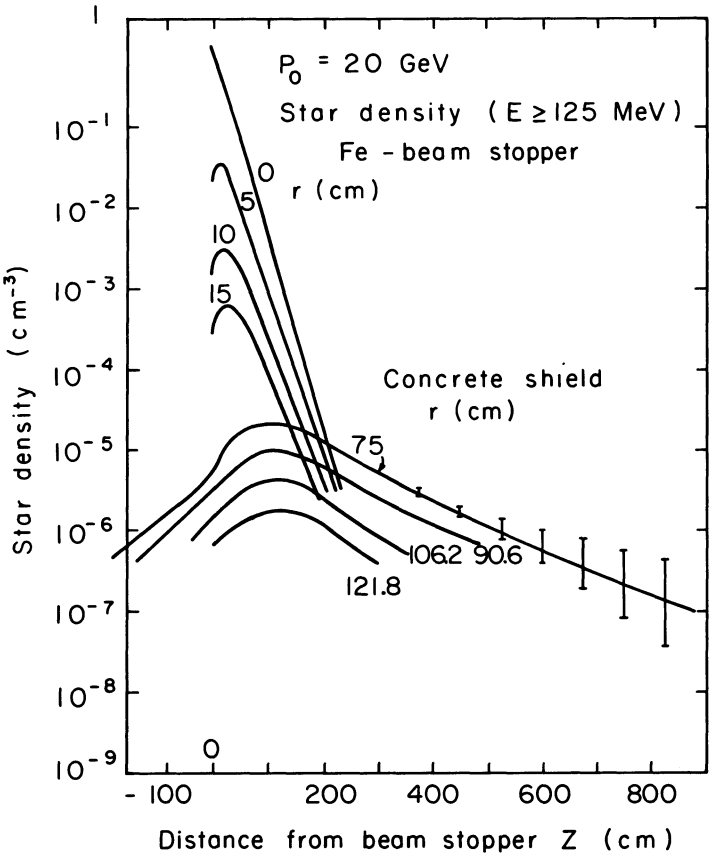

Fig. 9 Calculated star density (stars produced by strongly interacting particles of E ≥ 125 MeV) inside the iron beam stopper and inside the concrete shielding. The density is normalized to 1 star/cm^3 at r = 0 and Z = 0 in the beam stopper. The curves can also (approximately) be regarded as the corresponding flux densities, normalized to one incoming primary proton.

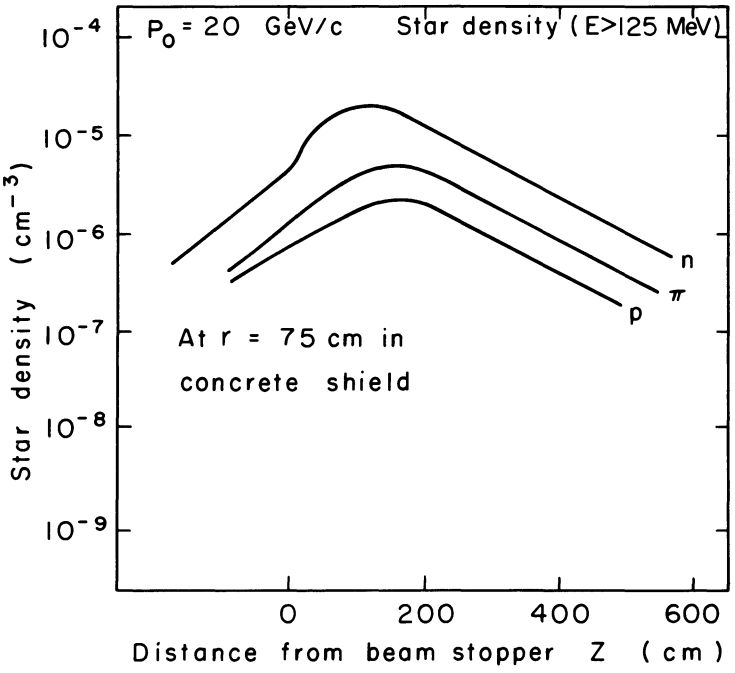

Fig. 10 Comparison of neutron, proton, and pion flux or star densities at r = 75 cm in the concrete shielding.

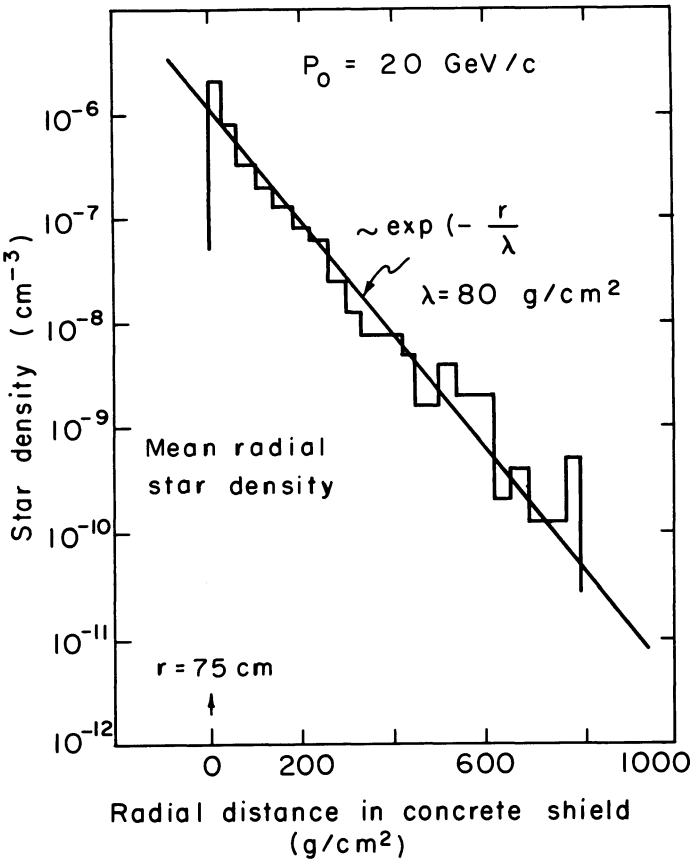

Fig. 11 Mean radial attenuation of the star density in the concrete shielding.

6. COMPARISON BETWEEN MEASURED AND CALCULATED PARTICLE FLUXES

The energy-dependent cross-sections of the activation reactions which we use:

$$\sigma_{Al,n} = \sigma_{[^{27}Al(n,\alpha)^{24}Na]} \ ,$$

$$\sigma_{Al,p} = \sigma_{[^{27}Al(p,3pn)^{24}Na]} \ ,$$

$$\sigma_{C,n} = \sigma_{[^{12}C(n,2n)^{11}C]} \ ,$$

$$\sigma_{C,p} = \sigma_{[^{12}C(p,pn)^{11}C]} \ ,$$

are given in Ref. 9. The neutron energy spectra $\phi_n(E)$ in and around the beam stopper and behind the shield are given below E = 100 MeV by the activation detector measurements. Individual spectra for points 1 to 21 continued above 100 MeV by the spectra from Fig. 7 for r = 100-120 g/cm^2, and for the points 30 to 40 by the spectra from Fig. 7 for r = 400-420 g/cm^2. The proton energy spectrum is assumed to have the form

$$\phi_p(E) = \frac{1}{3} \frac{(E + m_p)^2 - m_p^2}{(E + m_p)^2} \phi_n(E) \ ,$$

which is qualitatively in agreement with the calculated proton spectra in Fig. 6.

The number of nucleons contributing to the fluxes in the Monte Carlo calculation is

$$N_{MC} = \int_{125\ MeV}^{E_0} \left[\phi_n(E) + \phi_p(E)\right] dE$$

The number of nucleons contributing to the activation detector measurements is

$$N_{Al} = \int_{E_{thr(Al,n)}}^{E_0} \phi_n(E)\, dE + \int_{E_{thr(Al,p)}}^{E_0} \phi_p(E)\, dE$$

$$N_C = \int_{E_{thr(C,n)}}^{E_0} \phi_n(E)\, dE + \int_{E_{thr(C,p)}}^{E_0} \phi_p(E)\, dE \ .$$

We define the quantities

$$Q_{Al} = \frac{N_{Al}}{N_{MC}}$$

$$Q_C = \frac{N_C}{N_{MC}}$$

which are needed in order to compare the fluxes calculated in the Monte Carlo calculation with the measured fluxes.

The average Al and C activation cross-sections are:

$$\bar{\sigma}_{Al} = \frac{\int_{E_{thr(Al)}}^{E_0} [\phi_n(E)\,\sigma_{Al,n} + \phi_p(E)\,\sigma_{Al,p}]\,dE}{N_{Al}} = 38.8 \text{ mb}$$

$$\bar{\sigma}_{C} = \frac{\int_{E_{thr(C)}}^{E_0} [\phi_n(E)\,\sigma_{C,n} + \phi_p(E)\,\sigma_{C,p}]\,dE}{N_{C}} = 21 \text{ mb} \quad .$$

All these integrals can be evaluated by numerical integration.

The experimental particle fluxes given in Table 3 were obtained with $\bar{\sigma}_{Al} = 120$ mb and $\bar{\sigma}_{C} = 22$ mb. To compare the fluxes ϕ_{MC} obtained in the Monte Carlo calculation, with the measured ones ϕ_{Al} and ϕ_{C} given in Table 3, we convert the latter with the relations

$$\psi_{Al} = \frac{120 \text{ mb}}{\bar{\sigma}_{Al} \cdot Q_{Al}}\,\phi_{Al}$$

$$\psi_{C} = \frac{22 \text{ mb}}{\bar{\sigma}_{C} \cdot Q_{C}}\,\phi_{C} \quad .$$

This has been done for all points of the measurement. Table 5 gives the Monte Carlo fluxes ϕ_{MC} according to Fig. 9 for different positions around the beam stopper. The positions are characterized by the coordinates z and r. Table 6 gives the calculated $\bar{\sigma}_{Al}$ and $\bar{\sigma}_{C}$, and the calculated Q_{Al} and Q_{C} for each position, and compares the Monte Carlo fluxes ϕ_{MC} with the converted fluxes ψ_{Al} and ψ_{C}. In a second comparison the proton energy spectra were set equal to zero: $\phi_p(E) = 0$. Table 7 gives for this case the calculated $\bar{\sigma}_{Al}$ and $\bar{\sigma}_{C}$, Q_{Al} and Q_{C}, as well as the fluxes ψ_{Al} and ψ_{C}. Most numbers in Table 7 differ by less than 10% from the corresponding numbers of Table 6.

At the same time the fluxes obtained from the LOUHI spectra above 130 MeV are given. The fluxes as presented in the table are compatible with the <u>form</u> of the spectrum as in Fig. 9 and with <u>both</u> the ^{24}Na and ^{11}C responses as measured with the activation detectors.

Figure 11 shows that the calculated attenuation at large angles is compatible with an attenuation length of 80 g/cm^2. When the high-energy particle flux densities inside and outside the tunnel are normalized by multiplying by r^2, the apparent λ is 110 g/cm . This λ is in agreement with the values found for earth and concrete shielding in the CERN-LRL Rutherford shielding experiment.

The maximum radiation is measured on top of the shield at 80° with the beam direction. The dose equivalent at positions outside the shield is estimated from the flux densities to be 1.5 rem/h at positions 31 (770 g/cm^2) and 4.25 rem/h at position 37 (580 g/cm^2).

The radiation profile across the beam tunnel shows a minimum at the beam axis, and maximum values at 10° with the beam direction. Ten metres behind the 300 cm steel stopper, the dose-rate would be of the order of a couple hundred rem/h; in such geometry the two stoppers would be insufficient to control the access to a downstream area.

Table 5

Fluxes calculated at r_0 = 75 cm, and at $r = r_0 + 240$ cm and $r = r_0 + 320$ cm, in the concrete shield and for different Z positions. The fluxes at $r > r_0$ are obtained from

$$\phi(r) = \phi(r_0) \exp - \frac{(r - r_0)\ [g/cm^2]}{80}$$

The fluxes are normalized to one proton hitting the beam stopper.

Z (cm)	$\phi_{MC}(r_0)$	$\phi_{MC}(r_0 + 240)$	$\phi_{MC}(r_0 + 320)$
-120	1×10^{-6}		5×10^{-11}
30	1.2×10^{-5}		6×10^{-10}
60	1.7×10^{-5}		8×10^{-10}
70	2×10^{-5}	1.3×10^{-8}	1×10^{-9}
150	2×10^{-5}		1×10^{-9}
180	1.7×10^{-5}		8×10^{-10}
220	1×10^{-5}		5×10^{-10}
230	9×10^{-6}	6×10^{-9}	4.5×10^{-10}
330	4×10^{-6}		2×10^{-10}
430	$(1.8 - 2.2) \times 10^{-6}$		$(9 - 11) \times 10^{-10}$
530	$(7.5 - 14) \times 10^{-7}$		$(3.7 - 7) \times 10^{-11}$
830	$(4 - 40) \times 10^{-8}$		$(2 - 20) \times 10^{-12}$

The fluxes predicted by the Monte Carlo calculations differ from the experimental fluxes by more than a factor of 2 in only a few positions. The differences between the converted Al and C fluxes are smaller than a factor of 2, and both agree within about the same limit with the fluxes ϕ LOUHI.

Only the errors at positions 2, 6, and 7 are notably larger. These are the positions with $z \approx 0$. The reason for this disagreement is the poor statistical accuracy of the Monte Carlo results at locations perpendicular to the beam at the position where the primary proton hits the stopper. Efforts will be made to improve the Monte Carlo calculation in this respect.

Other systematic errors came from the fact that the energy spectra above E = 100 MeV cannot be expected to agree everywhere with the assumed ones, and from errors in the assumed activation cross-sections.

The agreement between experimental and calculated fluxes is already good enough for making an estimation of the shielding at the present stage. The predictions are better than the assumptions that can be made concerning beam losses in most of the practical cases. This latter uncertainty often demands higher safety factors for the shielding, than the uncertainties of the shielding estimation itself.

Table 6

Comparison of measured and calculated fluxes,
all normalized to one proton hitting the beam stopper

Position	Z (cm)	r (cm)	$\bar{\sigma}_{AL}$ (mb)	$\bar{\sigma}_{C}$ (mb)	Q_{Al}	Q_{C}	$10^{6} \times \phi_{MC}$	$10^{6} \times \psi_{Al}$	$10^{6} \times \psi_{C}$
2	60	55	35.1	21.5	3.9	2.3	17	92	126
3	220	55	30.3	21.5	3.6	2.2	10	11	25
4	150	40	33.6	21.3	4.6	2.9	20	20 20	32
5	150	40	31.9	27.3	4.0	2.5	20	26	45
6	30	75	37.1	21.3	5.4	2.9	12	40	59
7	30	75	37.5	21.3	6.6	2.8	12	41	76
8	180	75	34.7	21.3	4.2	2.5	17	21	34
9	180	75	30.7	21.6	3.3	2.2	17	32	42
10	330	75	33.0	21.5	3.7	2.3	4	5.5	8.1
11	330	40	38.8	21.2	5.3	2.7	4	2.4	3.7
12	330	40	39.5	21.2	5.8	3.0	4	1.9	2.9
13	330	75	33.2	21.3	4.1	2.6	4	5.0	8.4
14	530	75	33.3	21.3	4.1	2.6	0.75 - 1.4	1.3	2.15
15	530	40	36.5	21.3	4.4	2.5	0.75 - 1.4	1.05	1.65
16	530	0	38.8	21.1	5.7	3.0	0.74 - 1.4	0.75	1.2
17	530	40	39.4	21.1	5.7	2.9	0.74 - 1.4	0.75	1.25
18	530	75	37.3	21.1	5.2	2.9	0.74 - 1.4	1.1	1.75
19	-120	75	42.1	21.1	7.5	2.8	1.0	1.7	3.2
20	-120	75	43.5	21.0	8.5	3.4	1.0	1.4	2.3
							$10^{10} \times \phi_{MC}$	$10^{10} \times \psi_{Al}$	$10^{10} \times \psi_{C}$
31	70	R + 320	32.3	21.1	6.7	4.4	10	16.5	25
32	230	R + 320	30.3	21.1	6.7	4.7	4.5	5.5	8.6
33	330	R + 320	30.8	21.1	7.2	4.9	2.0	2.4	3.9
34	430	R + 320	33.9	21.0	7.8	4.8	0.9 2- 1.7	0.9	1.5
35	530	R + 320	38.6	21.0	7.5	4.1	0.32 - 0.7	0.36	0.55
36	830	R + 320	56.5	20.8	24.0	3.3	0.02 - 0.2	0.09	0.12
37	70	R + 240	36.2	21.0	7.5	4.4	130	47	63
38	230	R + 240	35.9	21.0	8.5	5.0	60	12	19.2
39	70	R + 320	36.4	21.1	7.4	4.3	10	6.0	9.2
40	230	R + 320	35.6	21.0	7.6	4.6	4.5	3.9	6.0

We may conclude that the Monte Carlo nucleon-meson cascade can be used, not only for simple but also for more complicated geometric situations, to predict with sufficient accuracy the shielding requirements for strongly interacting particles. The Monte Carlo method is possibly the most reliable of the methods known at present for estimating shielding requirements for future accelerators in the 200 to 500 GeV energy region.

Table 7

Comparison of measured and calculated fluxes, all normalized to one proton hitting the beam stopper. The proton energy spectra $\phi_p(E)$ are set equal to zero in the calculation of $\bar{\sigma}_{Al}$, $\bar{\sigma}_C$, Q_{Al}, and Q_C.

Position	Z (cm)	r (cm)	σ_{Al} (mb)	σ_C (mb)	Q_{Al}	Q_C	$10^6 \times \phi_{MC}$	$10^6 \times \psi_{Al}$	$10^6 \times \psi_C$	$10^6 \times \phi_{LOUHI}$
2	60	55	33.9	21.9	3.55	2.2	17	104	128	65
3	220	55	29.3	21.8	3.1	2.15	10	11.7	24.5	7.8
4	150	40	32.6	21.6	4.2	2.7	20	22.5	32.5	19
5	150	40	30.9	21.6	3.5	2.35	20	31.0	47.0	21
6	30	75	36.1	21.6	4.85	2.8	12	31.0	59.0	40
7	30	75	36.4	21.6	4.7	2.65	12	58.0	78.0	45
8	180	75	33.7	21.7	3.8	2.4	17	23.0	35.0	15
9	180	75	29.6	21.9	3.0	2.1	17	36.0	45.0	21
10	330	75	31.8	21.8	3.4	2.2	4.0	6.2	8.3	3.8
11	330	40	37.8	21.5	4.8	2.6	4.0	2.6	3.8	1.9
12	330	40	38.5	21.4	5.25	2.8	4.0	2.5	3.0	1.7
13	330	75	32.1	21.6	3.7	2.4	4.0	6.3	9.0	3.9
14	530	75	32.2	21.6	3.7	2.45	0.75 - 1.4	1.5	2.2	1.0
15	530	40	35.4	21.6	4.0	2.7	0.75 - 1.4	1.2	1.5	0.76
16	530	0	37.8	21.5	5.1	2.8	0.75 - 1.4	0.87	1.2	0.71
17	530	40	38.4	21.5	5.1	2.8	0.75 - 1.4	0.92	1.25	0.72
18	530	75	36.2	21.5	4.8	2.55	0.75 - 1.4	1.25	1.9	1.0
19	-120	75	41.2	21.5	6.0	2.75	1.0	2.1	3.2	1.6
20	-120	75	42.7	21.3	7.6	3.3	1.0	1.65	2.3	1.6
							$10^{10} \times \phi_{MC}$	$10^{10} \times \psi_{Al}$	$10^{10} \times \psi_C$	$10^{10} \times \phi_{LOUHI}$
31	70	R + 320	31.7	21.3	6.1	4.1	10	18.5	26.0	26
32	230	R + 320	19.7	21.4	6.2	4.4	4.5	6.1	9.3	9.0
33	330	R + 320	30.2	21.3	6.6	4.6	2.0	2.6	4.2	4.0
34	430	R + 320	33.2	21.3	7.1	4.6	0.9 - 1.1	1.0	1.5	1.5
35	530	R + 320	37.9	21.3	6.8	3.9	0.32 - 0.7	0.41	0.56	0.57
36	830	R + 320	56.2	21.4	21.0	3.4	0.02 - 0.2	0.01	0.11	0.012
37	70	R + 240	35.5	21.3	6.8	4.1	130	46.0	66.0	66.0
38	230	R + 240	35.2	21.2	7.7	4.7	60	14.0	20.5	20.0
39	70	R + 320	35.7	21.4	8.7	4.0	10	6.7	10.0	9.5
40	230	R + 320	34.9	21.3	7.0	4.3	4.5	4.2	6.2	6.2

Acknowledgements

The authors thank Dr. J. Baarli for his support of this work; E. Barbe, P. Coninckx, M. Nielsen and C. Renaud from the CERN Health Physics Group for their assistance with the activation measurements; and J. Dutrannois who helped to get the program KASTRA running at CERN. The help of A. Smith and N. Little (LRL, Berkeley) with "TELLY" computation, and of Dr. J. Routti in the use of the "LOUHI" program was very much appreciated. These computations of spectra were carried out during a year's stay of one of the authors (K.G.) with the Health Physics Department of the Lawrence Radiation Laboratory at Berkeley, California. Our thanks are also due to many members of the CERN Proton Synchrotron Machine Division for their assistance with the installation, calibration, and operation of the fast ejected proton beam.

REFERENCES

1) A. Citron, L. Hoffmann and C. Passow, Nuclear Instrum. Methods 14, 47 (1961).

2) A. Citron, L. Hoffmann, C. Passow, W.R. Nelson and M. Whitehead, Nuclear Instrum. Methods 32, 48 (1965).

3) J. Ranft, Nuclear Instrum. Methods 48, 133 (1967); ibid. 261 (1967); also CERN-MPS/Int. MU/EP 66-8, 1966.

4) T. Capone, J. Baarli, S. Charalambus, J. Dutrannois, J.Y. Freeman, K. Goebel, W.C. Middelkoop, T.R. Overton, A. Rindi and A.H. Sullivan, CERN Report DI/HP 71, 1965.

5) W. Gilbert, D. Keefe, J. McCaslin, H.W. Patterson, A.R. Smith, L.D. Stephens, K.B. Shaw, G.R. Stevenson, R.H. Thomas, R.D. Fortune and K. Goebel, UCRL-17941, Sept. 1968.

6) J. Ranft, CERN-MPS/Int. MU/EP 67-1, 1967; 67-6, 1967.

7) J. Ranft, MPS/Int. MU/EP 67-5, 1967.

8) K. Goebel, CERN Int. HP 68-60.

9) S. Charalambus, J. Dutrannois and K. Goebel, CERN DI/HP 90, 1966; J.B. Cumming, Ann. Rev. Nuclear Sci. 13, 261 (1963).

10) J. Routti, High-energy neutron spectroscopy with activation detectors, incorporating new methods for the analysis of Ge(Li) gamma-ray spectra and the solution of Fredholm integral equations (Ph.D. Thesis), UCRL-18514, April 1969.

11) J. Ranft and T. Borak, National Accelerator Laboratory Internal Report, NAL-FN 193 (21 Nov. 1969).